ARCHIVES OF MECHANICS
Arch. Mech. **75** (3), 365–396, 2023, DOI: 10.24423/aom.4212

Non-uniqueness of fracture parameter choice in simulations of concrete cracking at mesoscale level

B. KONDYS, J. BOBIŃSKI, I. MARZEC

Gdańsk University of Technology, Faculty of Civil and Environmental Engineering, 11/12 Gabriela Narutowicza Street, 80-233 Gdansk, Poland,
e-mail: jerzy.bobinski@pg.edu.pl (corresponding author)

In the paper a non-uniqueness of fracture parameter choice in simulations of cracking process in plain concrete specimens at mesoscale level under monotonic static loading is analysed. The Finite Element Method is used, where cracks are defined in a discrete way using interface cohesive elements with nonlinear material law including softening. The concrete mesostructure (such as: cement matrix, air voids, aggregates, and Interfacial Transitions Zones (ITZ)) is taken into account. Two benchmarks: Montevideo splitting test (MVD) as a main test and the three-point beam bending test (TPBT) as an auxiliary problem are simulated. Results from 2D calculations are compared with experimental outcomes, especially force-crack opening curves and crack patterns are carefully studied. In the MVD test, the mesostructure of a specimen is taken from X-ray micro-computed tomography scans of real samples. The issue of the proper selection of material parameters for cohesive cracks is investigated. The ambiguity of such a process is presented and discussed. It turns out the numerical simulations can give the same outcome for different values of material parameters. The influence of the selected material parameters and the friction coefficient on results (force–crack opening curves and crack patterns) is also analysed.

Key words: concrete mesostructured, Finite Element Method, discrete cracks, cohesive elements, wedge splitting test, beam under bending.

1. Introduction

Since cracking in concrete is an almost inevitable occurrence and it affects important mechanical properties of concrete, such as strength and stiffness, an accurate understanding of this phenomenon is the key to predicting how concrete elements will behave during loading [1]. Concrete, like other materials based on cementitious matrices, is a highly heterogeneous material. This makes the nature of the fracture, especially the crack propagation path, strongly dependent on the composition of the specimen. Therefore, to give a better insight into the cracking phenomenon the mesostructure of concrete should be considered. The mesostructure of concrete can be defined as the volume, shape and orientation of inclusions and voids inside the hardened cement matrix. A typical

concrete mesostructure consists of aggregates, cement matrix, air voids, interfacial transition zones (ITZ) and eventually other inclusions such as rebars or fibres [2]. Indivudual phases have different mechanical parameters. Especially important are ITZs that surround the inclusions and, through their low strength compared to a cement matrix, serve as attractors to cracks [3–7].

The cement-based material cracking mechanism is characterized as being quasi-brittle, which means that the stress in this material does not completely drop to zero as soon as it achieves its tensile strength [8] as in the case with perfectly brittle materials such as glass or ceramics. Reaching stresses equal to the tensile strength causes the creation of a fracture surface. Once a fracture surface has been formed owing to loading, the crack will continue to propagate until strain energy is completely dissipated. In other terms, despite the material's weakening due to cracking, it can still transfer tensile stresses. The behaviour of the material during the fracture propagation can be described in terms of the fracture energy G_F, which is usually assumed as a material constant defined as the amount of energy required to a fully nucleated unit area of the crack surface [9].

The fracture energy is a fundamental material parameter for the numerical modelling of fracture phenomena for most constitutive laws both for continuous and discontinuous approaches [10–12]. The continuous approach, or in other words the smeared crack approach, describes the crack as a continuous strain band, the physical interpretation of which are the areas of microcracks that appear before the formation of a visible macro crack. This method is widely used [13–19] and has the great advantage of a relatively low computational effort and the possibility to use standard finite element codes. In the discrete approach, cracks are introduced explicitly as discontinuities in the model. That approach allows a very accurate numerical representation of the crack paths in comparison to images obtained in experimental tests [7, 20, 21].

Experimental tests to determine fracture energy can be divided into two basic categories: direct and indirect. In the direct approach, a tensile load is applied to the specimen e.g., an uniaxial tension test (UTT/DTT) [22, 23], a compact tension test (CT) [24] or a modified compact tension test (MCT) [25]. Direct methods are used relatively infrequently, due to specimen's slippage in the grips and localised disturbances in the stress distribution (especially for UTT) and in the case of CT/MCT due to the requirement of the appropriate shaping of specimens, which makes it particularly difficult to test specimens with coarse aggregate.

Indirect approaches can be subdivided into three main groups:

- Direct splitting: the double punch test (DPT/Barcelona test) [26], prismatic or cylindrical Brazilian direct splitting [27, 28] and variations of this test e.g., the flattened Brazilian disk test (FBD) [29] or the cracked chevron notched Brazilian disk test (CCNB) [30, 31].

- Wedge splitting: the wedge splitting test (WST) [32, 33], the Montevideo splitting test (MVD) [34, 35] or the double edge notched wedge splitting test (DEWS/DEWST) [36].
- Bending: the three-point bending test (TPBT/3PBT) [37], the four-point beam bending test (FPB) [38] or the semi-circular specimen bending test (SCB) [30].

Of all the aforementioned tests, WST and TPBT tests are currently widely performed, for which recommendations have been developed that allow reproducible and reliable results.

The current level of development of computational methods allows for accurate modelling of crack propagation phenomena in highly heterogeneous materials such as concrete. The increase in modelling accuracy implies the need to consider an even greater number of material parameters, both those that have a physical interpretation and those that have only numerical meaning. When modelling crack propagation in concrete specimens at the mesoscale level, it is necessary to consider not only the real shape of the mesostructure but also the material parameters of the various phases of which the concrete is composed. The assumed values play an important role and they may affect the obtained response significantly. The determination of parameters for each phase is a complicated issue. There are also no uniform guidelines for testing mechanical properties for certain phases e.g., ITZs. For some simulation types, it may be necessary to consider secondary effects such as friction or the loading rate. As a result, several values are chosen using the rules of thumb. The main method of determining the mechanical parameters of the individual phases is calibration, usually involving a procedure to achieve convergence with experiments for the overall model response, e.g., the force-crack mouth opening displacement (CMOD) or force-displacement plots and comparing the resulting cracked image with the experimental outcomes [20, 39, 40].

The aim of the paper is to investigate the influence of the choice of fracture parameters on the obtained results. The Finite Element Method (FEM) is used with interface cohesive elements to describe cracks. 2D plane stress simulations are performed. The determination of two principal cracks' growth parameters: the strength and softening description including the fracture energy in both phases are carefully studied. Special attention is paid to the uniqueness of the assumed set of parameters derived from the compliance criterion with experiments. Two experiments with the dominated mode I failure mode is numerically simulated: a wedge splitting test and a three-point bending test. A real mesostructure is considered. Results from numerical calculations (force-displacement curves and crack patterns) are compared with experimental outcomes.

This paper is a continuation of our previous publication [41] in which the simplified Montevideo splitting test was also numerically studied. In order to

investigate the influence of some essential parameters on the obtained force-displacement curves and crack patterns, parametric simulations were executed (while unchanged values of the remaining parameters). The main goal of this study is to analyse the issue of the uniqueness (or rather nonuniqueness) of the choice of the material parameter set required to obtain physically sound (consistent with the experiment) results, when mesostructure of concrete is considered. As a result, a family of parameter set is found for each of two analysesd boundary-value problems. In addition, a mesh insensitivity for the first benchmark is also examined.

The paper is organized as follows. The numerical model definition and the mesh preparation procedure are presented in Section 2. Next in Section 3 paper presents the constitutive laws used to describe the models. Details of the experiments, input data, simulation results, parametric studies and final the parameter choice set can be found in Sections 4 (wedge splitting test) and 5 (three-point bending test). The final Section 6 provides a summary and conclusions.

2. Definition of models

Two boundary value problems were studied: a simplified Montevideo splitting test (Fig. 1) and a three point bending test (Fig. 2). A finite element method using Abaqus software was chosen to perform the simulations. Based on micro-CT

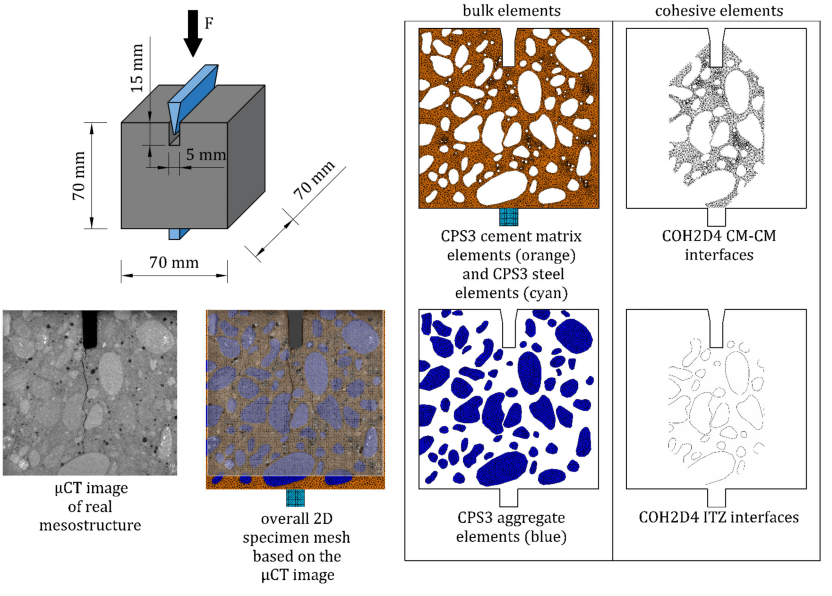

FIG. 1. Simplified Montevideo splliting test: geometry, boundary conditions, FEM model and a scheme for preparation of a numerical model based on micro-CT scan.

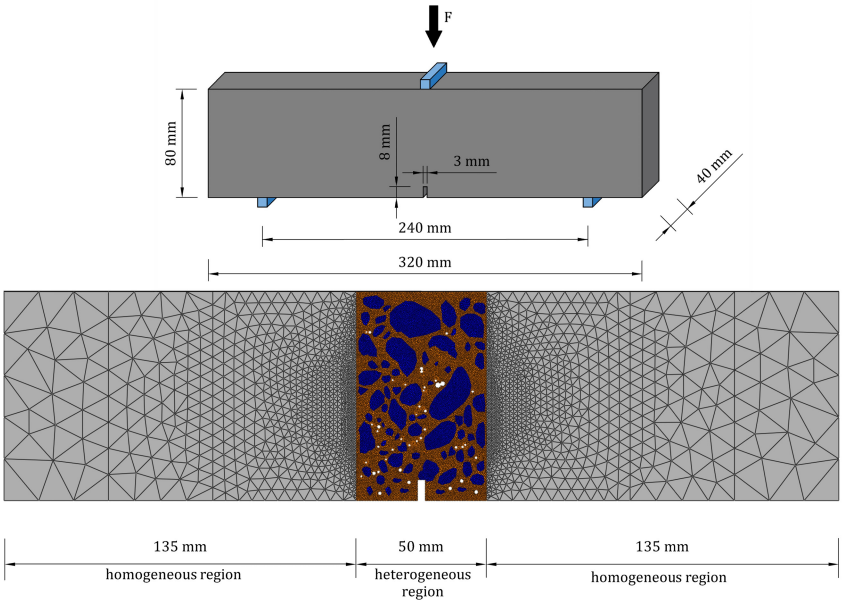

FIG. 2. Three-point bending test: geometry, boundary conditions and FEM model.

scans two-dimensional computational models were created in the plane stress state. In the case of the wedge splitting, the mesostructure was considered over the entire surface of the model (Fig. 1), while in the case of the TPBT, a two-scale model was used – the mesostructure was defined only in the central part of the beam (Fig. 2), the rest of the beam was modelled as homogeneous. Aggregates and air pores in microstructure images were identified visually, and their borders were defined manually as a set of straight edges, similarly as in [20]. It allowed to define indivual aggregates and the cement matrix region in the specimen. Three-node 2D plane stress elements (CPS3) were selected as the bulk elements. Zero-thickness four-node 2D cohesive elements (COH2D4) were inserted into the existing bulk finite element mesh (Fig. 1) by using the modified DEIP script [42], in regions where cracking was expected to occur. The restriction of the area with defined cohesive elements on the one hand, allowed the reduction of computational effort and on the other hand, avoided the numerical problems in wedge splitting simulations caused by the application of the isotropic constitutive law at the areas of the complex stress state (significant shear or compressive stresses). The model distinguishes between two types of cohesive elements – to simulate cement matrix cracking (CM-CM) and cracking in ITZs. Due to the high strength and stiffness of the aggregate grains, the probability of crack propagation through this phase of the mesostructure is negligible (which is confirmed by the experimental cracking patterns), which is the reason that no interfaces were inserted between the bulk aggregate elements.

3. Constitutive laws

3.1. Bulk concrete

The behaviour of the solid bulk continuum of all phases of the concrete mesostructure (cement matrix, and aggregate) and homogenous concrete as well as auxiliary steel elements was assumed to be linear elastic. The relationship between stresses $\boldsymbol{\sigma}$ and strains $\boldsymbol{\varepsilon}$ in these elements was described according to Hooke's linear-elastic law by means of Young's modulus E and Poisson's ratio ν. For a two-dimensional problem, this relationship can be written as follows:

$$\begin{bmatrix} \sigma_{11} \\ \sigma_{22} \\ \sigma_{12} \end{bmatrix} = \frac{E}{1-\nu^2} \begin{bmatrix} 1 & \nu & 0 \\ \nu & 1 & 0 \\ 0 & 0 & \frac{(1-\nu)}{2} \end{bmatrix} \begin{bmatrix} \varepsilon_{11} \\ \varepsilon_{22} \\ \varepsilon_{12} \end{bmatrix}. \tag{3.1}$$

3.2. Discrete crack

To introduce discrete cracking to the model the formulation of HILLEBORG *et al.* [9] was used. In the Hilleborg fictitious crack model, a material point in the path of crack expansion is assumed to be in one of three possible states: (1) the state of elastic behaviour, (2) the state of cracking (microcracks form, the stiffness of the material in the microcrack region decreases) and (3) the state of complete absence of stress transfer. The behaviour of the microcrack region can be described by the traction-separation law in which the concept of traction stress opposing the process of the crack mouth opening (separation) is introduced. Therefore, in the one-dimensional, pure tension case, the main idea of this approach can be represented as follows. The value of traction stress t_n is variable, initially this stress is equal to the normal stress σ_n interacting at the notch tip, but when stress value reaches the tensile strength of the material f_t, weakening occurs, which means that it gradually loses its ability to transmit stress across the crack. The phenomenon of softening is correlated with crack opening and can be described by the following equation

$$t_n = \begin{cases} \sigma_n, & \sigma_n \leq f_t, \\ f(\delta), & \sigma_n > f_t, \end{cases} \tag{3.2}$$

where $f(\delta)$ is the softening function dependent on the crack opening δ. Hilleborg's fictitious crack concept can be easily implemented in the FEM numerical model by using e.g., cohesive elements (Fig. 3).

In the general two-dimensional case, the stress vector contains a shear stress component in addition to the normal stress component, so the traction-separation law can be formulated as follows

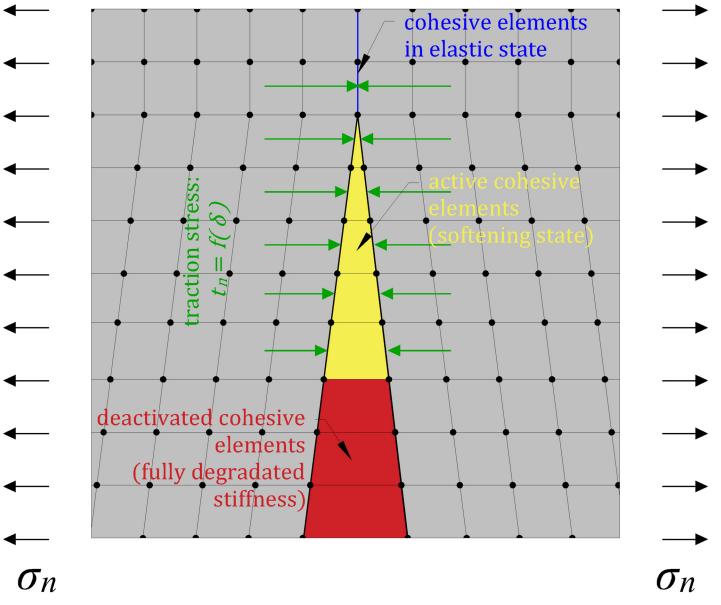

FIG. 3. The idea of cohesive elements behaviour in terms of traction-separation law in a FEM model.

$$\begin{bmatrix} t_n \\ t_s \end{bmatrix} = \begin{bmatrix} k_n & 0 \\ 0 & k_s \end{bmatrix} \begin{bmatrix} \delta_n \\ \delta_s \end{bmatrix}, \tag{3.3}$$

where t_n and t_s are normal and shear in tangential direction tractions, respectively, k_n and k_s are interface stiffness in the corresponding directions, δ_n and δ_s are the relative displacements related to the directions of traction.

The quadratic nominal stress criterion is assumed as the crack initiation criterion:

$$\left\{ \frac{\langle t_n \rangle}{t_{n0}} \right\}^2 + \left\{ \frac{t_s}{t_{s0}} \right\}^2 = 1, \tag{3.4}$$

where t_{n0}, t_{s0} are the critical stress (strength) in the normal and tangential direction, respectively and $\langle\,\rangle$ denotes the Macaulay bracket which represents the ramp function:

$$\langle \mathrm{x} \rangle = \begin{cases} 0, & x < 0, \\ x, & x \geq 0. \end{cases} \tag{3.5}$$

Equation (3.5) implies that crack initiation cannot occur due to compressive (normal) stresses. To describe damage under a combination of normal and tangential shear deformations across the interface, the effective relative displacement δ_m is introduced:

$$\delta_m = \sqrt{\langle \delta_n \rangle^2 + \delta_s^2}. \tag{3.6}$$

As a consequence of Eq. (3.6) negative normal relative displacements shall not be considered in the description of the crack propagation when the initiation criterion described by Eq. (3.4) is fulfilled in a particular cohesive element, the stiffness degradation process of that element begins. To describe this softening effect scalar damage variable D is used:

$$\begin{aligned} k_n &= (1-D)k_{n0}, \\ k_s &= (1-D)k_{s0}, \end{aligned} \tag{3.7}$$

where k_{n0} and k_{s0} denote the initial interface stiffness in normal and tangential directions, respectively. Depending on the material behaviour, the evolution of the parameter D can be described by different curves. For heterogeneous quasi-brittle materials, the bilinear [43] or exponential curve [44] is most commonly used. In this paper the numerical model with an exponential softening curve defined using effective relative displacements is assumed:

$$D = \begin{cases} 1 - \left\{\dfrac{\delta_m^0}{\delta_m^{\max}}\right\}\left\{1 - \dfrac{1-\exp\left[-\alpha\left(\frac{\delta_m^{\max}-\delta_m^0}{\delta_m^f-\delta_m^0}\right)\right]}{1-\exp(-\alpha)}\right\}, & \delta_m^{\max} \le \delta_m^f, \\ 1, & \delta_m^{\max} > \delta_m^f, \end{cases} \tag{3.8}$$

where δ_m^0 means the effective, relative displacement at the crack initiation, δ_m^f is the effective relative displacement at the complete stiffness degradation, $\delta_m^{\max}$ stands for the maximum effective relative displacement obtained during the

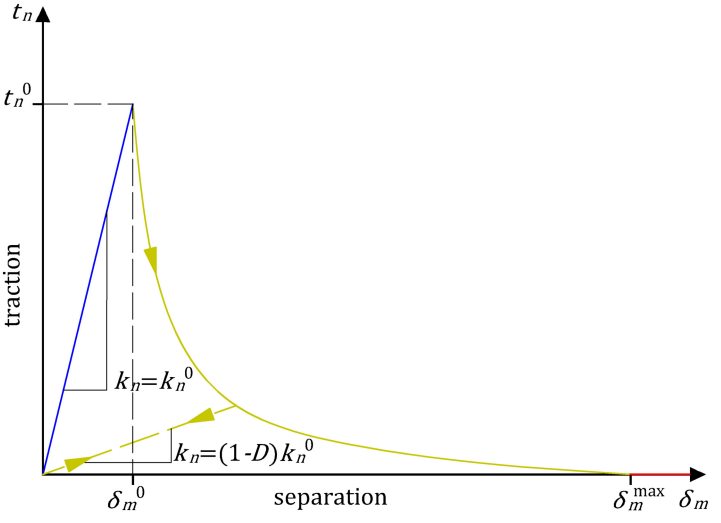

FIG. 4. Exponential traction-separation law curve for mode I failure.

loading history and α is the non-dimensional material parameter that controls the rate of damage evolution. Figure 4 presents traction – relative displacement curve in a normal direction under the assumption of zero shear relative displacement δ_s.

4. Simplified Montevideo Splitting Test

4.1. Experiment

The standard WST is based on pushing a rigid steel wedge into a pre-prepared notch in a cubic specimen. The inclination of the wedge creates horizontal force components that cause splitting of the specimen and therefore concentration of tensile stress, which creates a nearly pure mode-I state in the crack tip. By using small cubic samples, it is also possible to carry out the test on specimens prepared for compressive strength testing or taken directly from larger elements or existing structures. An important issue in WST is the presence of a significant vertical component of a force that is due to friction between the wedge and notch. To reduce this problem, special equipment is used (i.e. frames with bearing rollers or additional steel spacers and cylinders), but this requires an additional widening of the notch.

Therefore, it is particularly interesting to make an attempt to develop a suitable simplification of the standard WST, such as the MVD, where the wedge is applied directly to the notch. In the original version of the Montevideo splitting test proposed by Segura-Castillo *et al.* [34] extra steel profiles are placed between the specimen and the wedge. In the version of the test setup proposed by Skarżyński *et al.* [35] the load is applied directly to the concrete specimen, so for the purposes of this work this approach is referred to as "simplified MVD". Resignation of additional equipment simplifies the preparation and testing of the specimen, but at the expense of having to consider the non-negligible vertical stresses occurring from friction between the wedge and the steel profiles/concrete specimen when interpreting the results.

The experimental simplified MVD tests were carried out on cubic specimens with dimensions $70\times70\times70$ mm supported along their entire length by a 7×7 mm steel flat bar. An initial notch was placed in the centre of the upper surface of the specimen. The dimensions of the notch were 15 mm high and 5 mm wide. The concrete mix consisted of cement CEM II/A-LL 42.5R (300 kg/m^3), fly ash (70 kg/m^3), aggregates (1830 kg/m^3), superplasticizer (1.8 kg/m^3) and water (15 kg/m^3). Aggregates were divided into three main grain fractions: sand – maximum grain size equal to 2 mm (40.2% overall weight of aggregates), fine gravel – grain size in the range of 2 mm and 8 mm (23.5%) and coarse gravel with the maximum grain size equal 16 mm (36.3%). Compressive, tensile, and

Table 1. Concrete mechanical parameters from experimental test.

Mechanical test type	Type of sample	Number of samples	Average density [kg/m^3]	Standard deviation [kg/m^3]	Average stress [MPa]	Standard deviation [MPa]
Compressive strength	Cube 150×150×150 [mm]	6	2359.2	15.26	47.60	1.66
Tensile strength	Cube 150×150×150 [mm]	6	2361.1	6.99	3.46	0.19
Flexural strength	Beam 150×150×600 [mm]	6	–	–	3.60	0.20

flexural tensile tests were carried out to determine the material parameters of the concrete; the results are summarised in Table 1.

The specimen was subjected to the quasi-static simplified MVD test using a steel wedge with an inclination of 10° mounted in the Instron 5569 machine. The vertical force – crack mouth opening displacement (F-CMOD) (Fig. 5) relationship was recorded during the test. After the splitting test, damaged specimen scanning was performed with the Skyscan 1173 micro-tomograph, resulting in 3 different cross-section images (S1–S3) showing the internal mesostructure of the specimen and the cracking path (Fig. 6).

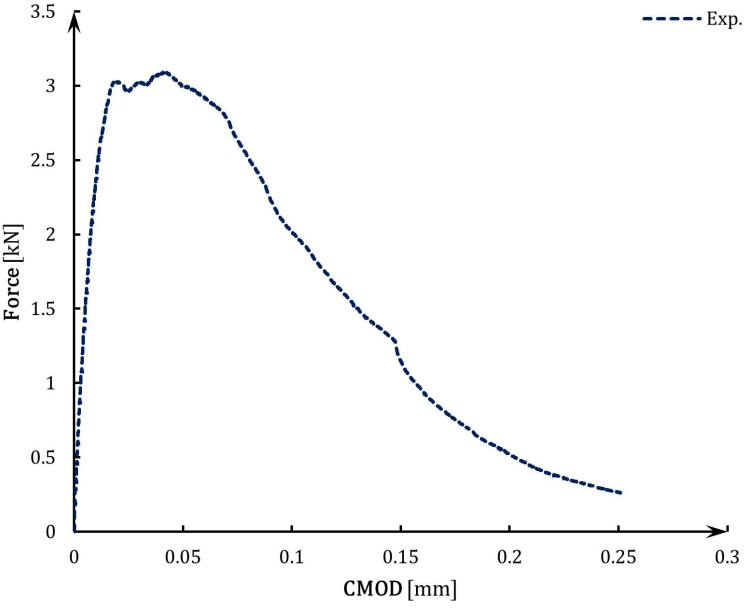

Fig. 5. Experimental F-CMOD curve for simplified MVD test.

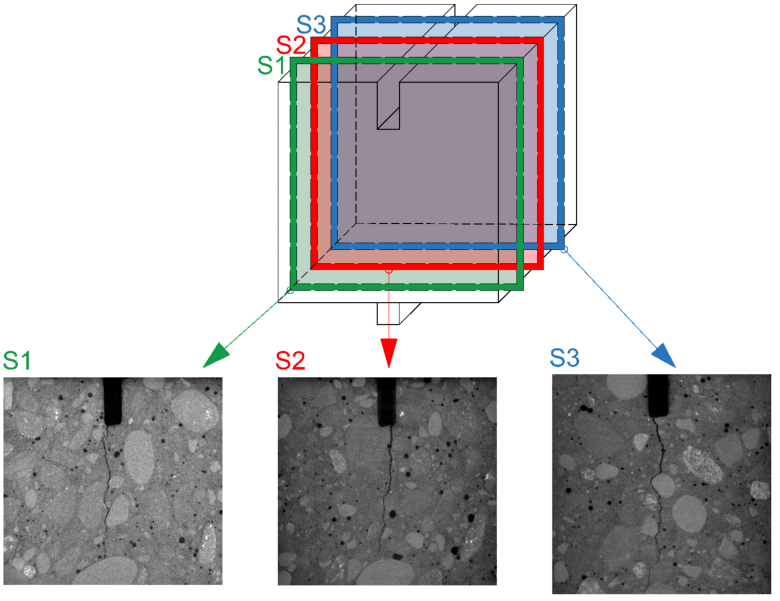

FIG. 6. Localization scheme of scan sections and mesostructure images for sections S1–S3.

4.2. Input data

The input parameters were established on the basis of experimental and preliminary parametric studies. Young's modulus of the homogeneous concrete, determined from experimental tests, was 34 GPa, while the bulk stiffness of the individual phases – the cement matrix and the aggregate – was determined from the average volume of these phases in the entire sample volume. The modulus of elasticity of steel and Poisson's ratios for all elastic phases were taken as the basic values for these materials (Table 2).

TABLE 2. Input parameters for bulk elements – MVD test.

Material parameter	Aggregate	Cement matrix	Steel
E [GPa]	40	20	200
ν [–]	0.2	0.2	0.3

The experimental average tensile strength of the concrete $f_t = 35$ MPa was chosen as the initial parameter for describing the cohesive zone – this value was taken as the strength of the CM-CM interfaces $f_{t,n,CEM} = f_{t,s,CEM} = f_{t,CEM} = 3.5$ MPa. As the recommendations for the tensile strength of the ITZ $f_{t,ITZ}$ in relation to the strength of the cementitious matrix $f_{t,CEM}$ in the current literature are not clear – the ratio $f_{t,ITZ}/f_{t,CEM}$ was considered to be around

0.4 to 0.8 [20, 45–47] – this parameter was chosen in the process of the parametric study. The final assumption for ITZ tensile strength was $f_{t,n,ITZ} = f_{t,s,ITZ} = f_{t,ITZ} = 0.5 f_{t,CEM} = 1.75\,\mathrm{MPa}$. Parametric studies were also executed to obtain the value of fracture energy. The calculations established a value of $G_{F,CEM} = 70\,\mathrm{N/m}$, while a value of $G_{F,ITZ} = 35\,\mathrm{N/m}$. The final values of the relative displacement $\delta_m^{\max}$ necessary to define the exponential softening curves, were determined from the previously adopted f_t and G_F. Parameters without direct physical interpretation, i.e. the initial stiffness of the cohesive elements k^0 and the exponential parameter α, were taken from Trawiński *et al.* [20] as $k_n^0 = 10^6\,\mathrm{MPa/mm}$ and $\alpha = 7.5$, respectively. Due to the fact that there is an almost pure tension condition at the tip of the crack it was assumed that the parameters of the cohesive elements in the tangential and normal directions would remain the same. The material parameters of the cohesive elements are summarised in Table 3. The default value of the friction coefficient $\mu = 0.5$ was set.

Table 3. Input parameters for cohesive elements – MVD test.

Material parameter	CM-CM	ITZ
k_n^0, k_s^0 [MPa/mm]	10^6	10^6
$f_{t,n}$, $f_{t,s}$ [MPa]	3.5	1.75
α [–]	7.5	7.5
G_F [N/m]	70	35

4.3. Primary results

Three samples with different mesostructure patterns were analysed, and the sample names corresponded to the names of the mesostructure sections (S1–S3). A quasi-static analysis with implicit integration in Abaqus/Standard was performed. At this point, it is worth noting that, in order to avoid point contact between the wedge and the notch, the contact area was increased in the numerical model by making a bevel parallel to the inclination of the wedge at a height of 1/3 of the notch. Both the F-CMOD responses and the corresponding outline paths with the input mesostructure scans were investigated and compared. As can be seen in Fig. 7, the numerical models exhibit slightly more brittle behaviour compared to the experimental F-CMOD plots. The best compliance in tensile strength was obtained for the model S2. For models S1 and S3, and also for the averaged diagram (from three sections with the same weights), a noticeably higher tensile strength of the specimen was obtained in comparison with the experimental results. In terms of the correspondence of cracking paths between numerical simulations and experiment, a satisfactory convergence can be observed (Fig. 8). The largest inconsistency was observed for model S1, where, due to the

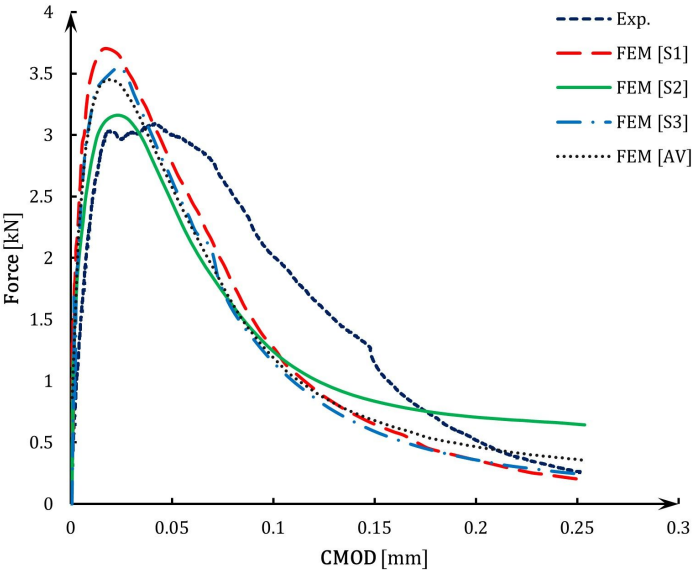

FIG. 7. Primary F-CMOD curves for models S1–S3 and averaged diagram in comparison to experimental outcomes.

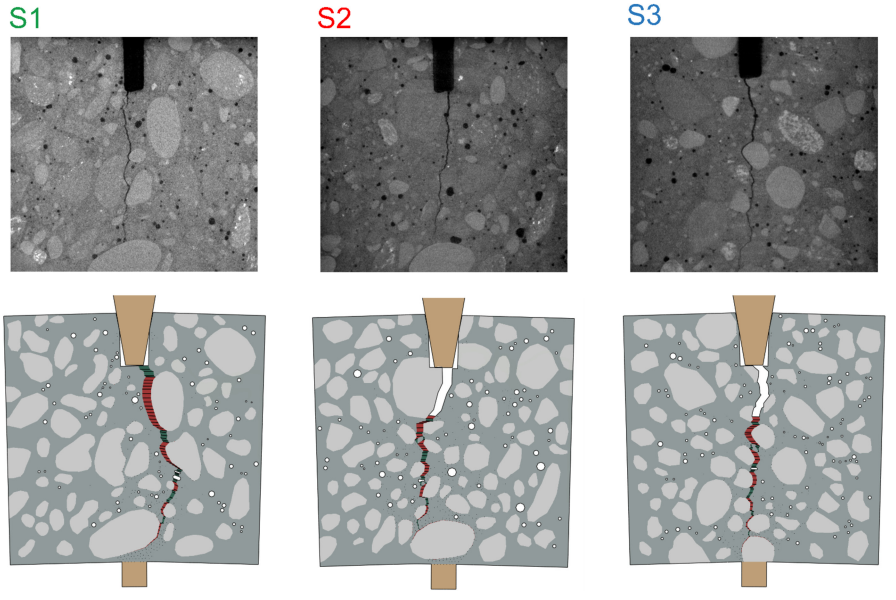

FIG. 8. Comparison of cracking images obtained experimentally and numerically for all mesostructures considered (S1–S3).

presence of a large aggregate grain near the notch, the ITZ surrounding this grain attracted the crack and altered its further propagation. During the parametric

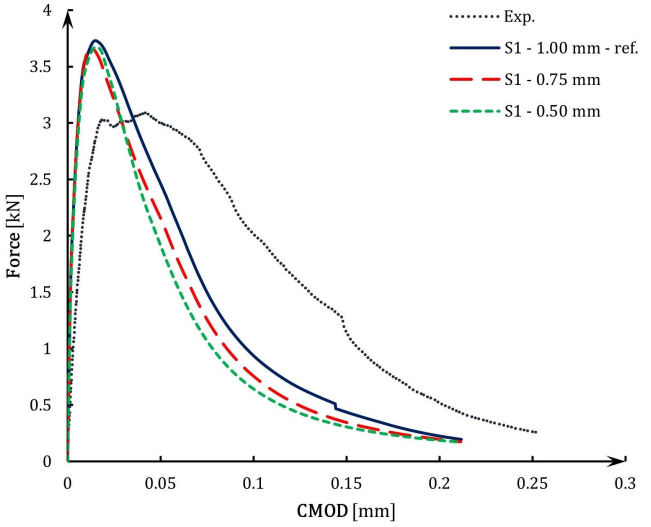

FIG. 9. *F*-CMOD curve for MVD test and FE mesh independence study for S1 section with comparison to experimental outcome.

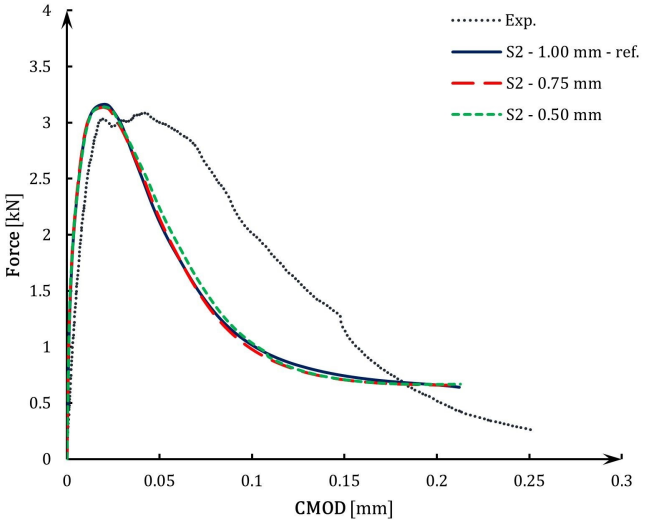

FIG. 10. *F*-CMOD curve for MVD test and FE mesh independence study for S2 section with comparison to experimental outcome.

study, it was not possible to establish greater convergence between the numerical calculations and the experimental results using the approach described earlier. This is probably due to the fact that, in reality, the crack should be considered as a surface, since its final trajectory is influenced by the mesostructure present

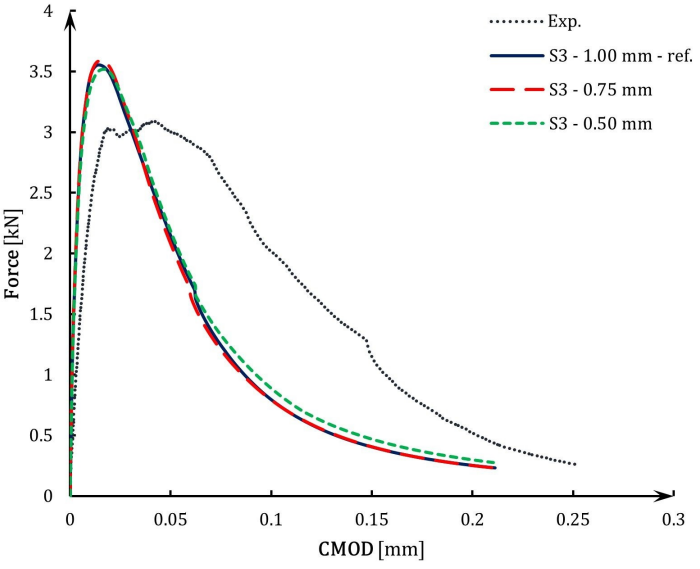

FIG. 11. F-CMOD curve for MVD test and FE mesh independence study for S3 section with comparison to experimental outcome.

in its entire volume, and therefore the consideration of a 3D model may bring a significant increase in the accuracy of the calculations and is a natural next step in the development of the presented method.

Additionally, a series of simulations were carried out to investigate the effect of the mesh independence on the numerical results. Calculations were performed for all S1, S2 and S3 sections with 3 different meshes with the minimum finite element size of 0.5 mm, 0.75 mm and 1 mm. The mesh independence with respect to F-CMOD relationships (Figs. 9–11) and the cracking paths (Figs. 12–14) were checked. The satisfactory convergence of these two criteria was obtained for all results. Obtained curves were practically identical, only some minor discrepancies

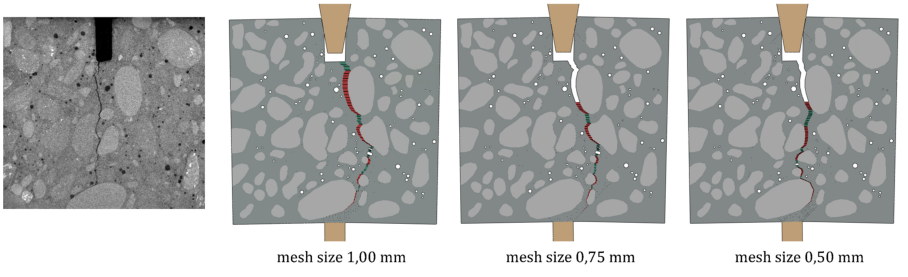

FIG. 12. Experimental crack pattern vs numerical crack patterns for section S1 and different FE mesh sizes.

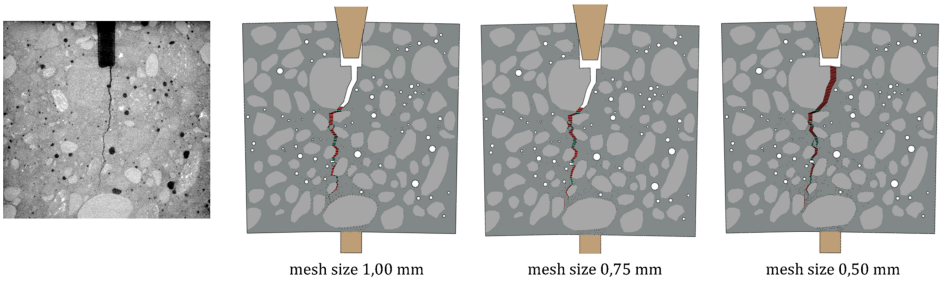

FIG. 13. Experimental crack pattern vs numerical crack patterns for section S2 and different FE mesh sizes.

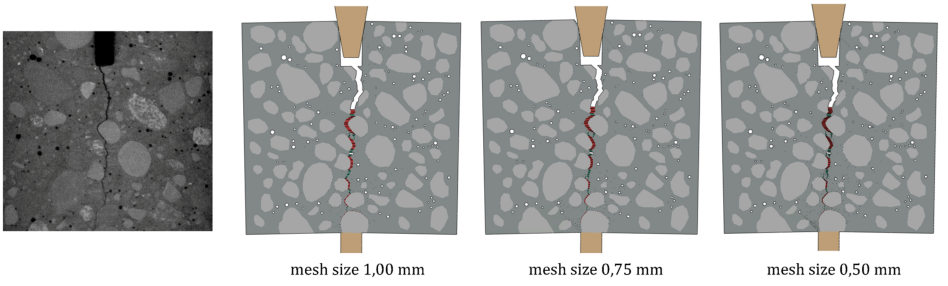

FIG. 14. Experimental crack pattern vs numerical crack patterns for section S3 and different FE mesh sizes.

were observed for the section S1. The largest difference in the crack trajectory was achieved for the section S1 and the FE mesh size 0.5 mm (comparing to other mesh sizes) in the half bottom part. The cracks in sections S2 and S3 were very similar for all meshes. Therefore, to reduce the computational cost, the FE mesh size 1 mm was found sufficiently precise and it was used as a default one in calculations.

4.4. Parametric study

In order to verify the assumptions previously made, a series of parametric simulations were carried out in which the influence of the mechanical parameters of the ITZs in relation to the parameters of the cement matrix and the influence of frictional forces were mainly investigated. An analysis was carried out on the section with the best consistency of results – S2. As can be seen in Figs. 15 and 16, since the crack mainly runs through the ITZs, changing the parameters characterising these zones significantly affects the response of the whole model, which is in line with the primary assumptions. This is also noticeable in the cracking paths – a relative increase in the parameters of the ITZs changes the trajectory of the crack (Figs. 17 and 18).

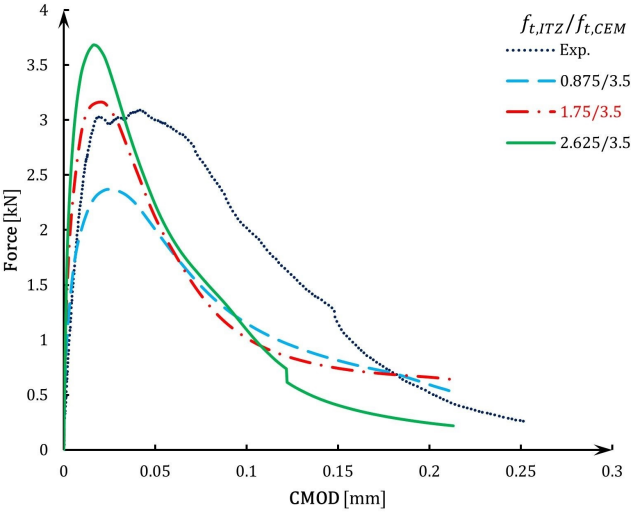

FIG. 15. F-CMOD curve for MVD tensile strength parametric study with comparison to experimental outcomes.

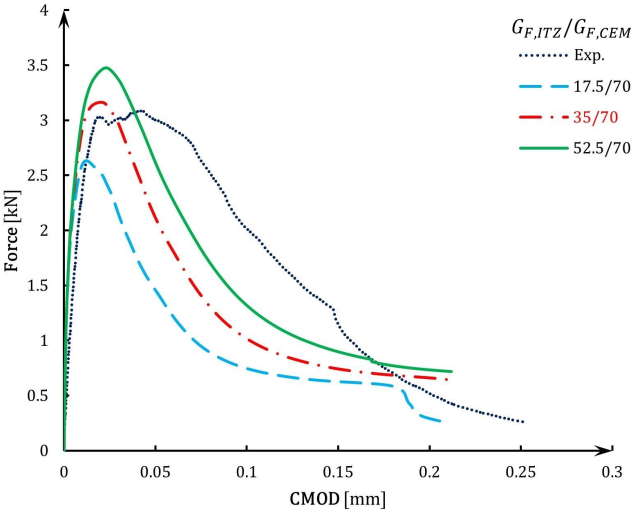

FIG. 16. F-CMOD curve for MVD fracture energy parametric study with comparison to experimental outcomes.

As previously mentioned, the MVD test is characterised by non-negligible frictional forces, so a friction coefficient had to be assumed for the simulation to proceed properly. Due to the lack of experimental data to determine this coefficient precisely, the recommended value was adopted. According to studies by RABBAT and RUSSEL [48], the friction coefficient μ for the steel-concrete interface has a value between 0.57 and 0.7. On the basis of the parameter studies, the

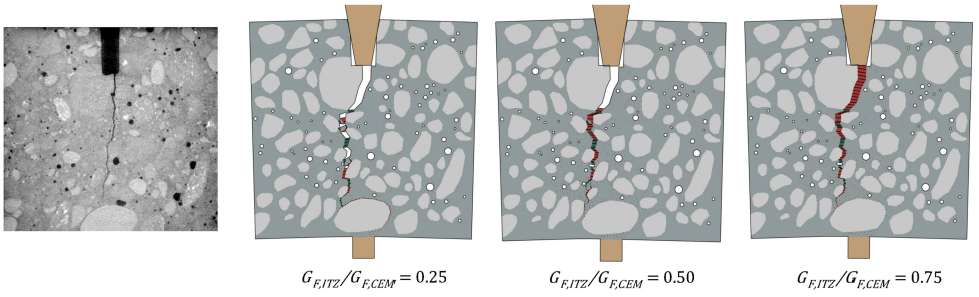

FIG. 17. Experimental crack pattern vs comparison of crack patterns for different $G_{F,ITZ}/G_{F,CEM}$ ratios.

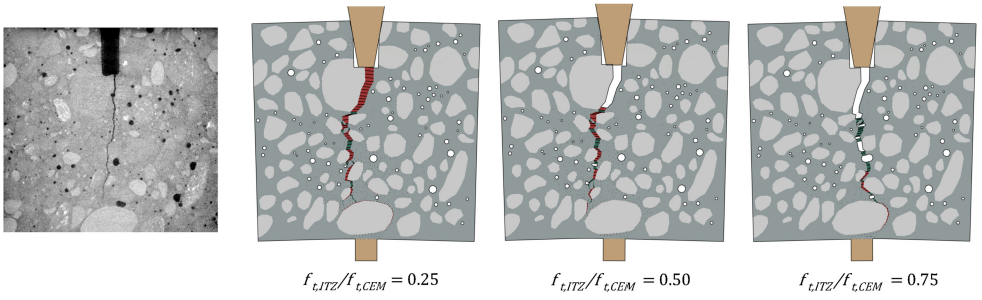

FIG. 18. Experimental crack pattern vs comparison of crack patterns for different $f_{t,ITZ}/f_{t,CEM}$ ratios.

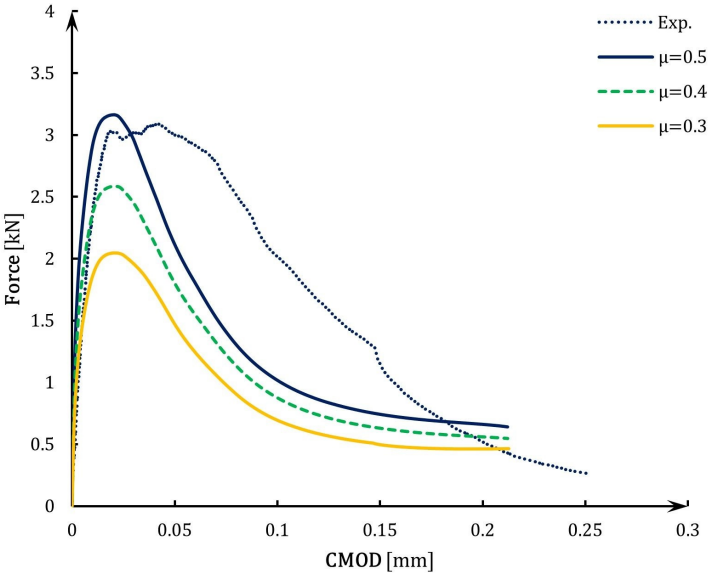

FIG. 19. F-CMOD curve for MVD friction coefficient parametric study with comparison to experimental outcomes.

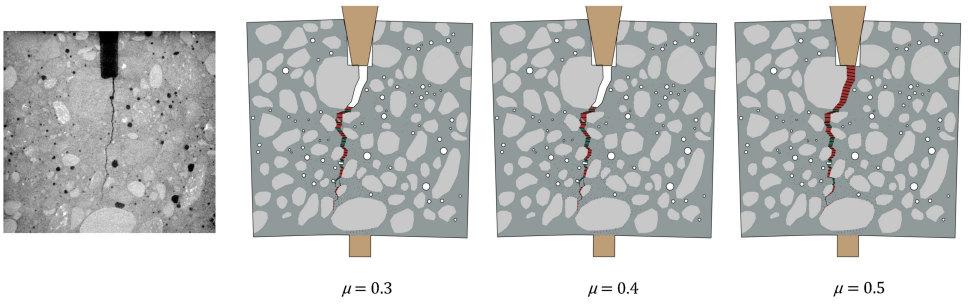

FIG. 20. Experimental crack pattern vs comparison of crack patterns for different friction coefficient definition.

final value of the coefficient was determined to be equal $\mu = 0.5$, a value slightly lower than recommended and this is most likely due to the artificial increase of the contact area by bevelling the edges of the notch in the numerical models. As expected, friction strongly influences the numerical results, especially in terms of the F-CMOD response (Fig. 19). Decreasing friction naturally results in a decrease in the vertical force. In the case of cracking images, subtle differences in the crack path can be noticed, but the overall trajectory remains the same (Fig. 20).

4.5. Choice of parameter set

The use of complex models and material laws almost always results in the need to make assumptions about a certain set of model parameters. If, in addition, these parameters are partially dependent on each other, as is the case for tensile strength and fracture energy in a cohesive model, there is a high chance that similar final results can be obtained for different (even strongly different) parameter sets. This section aims to illustrate this phenomenon using the MVD test as an example. In this test, as mentioned in Section 4.2, the tensile strength and the fracture energy for the ITZ is assumed to be half that of the cement matrix, as the actual experimental obtained values are not known.

The first set of parametric results presents an approach in which $f_{t,CEM}$ was assumed to remain constant, while values $G_{f,CEM}$ were adjusted and the ITZs parameters $f_{t,ITZ}$ and $G_{f,ITZ}$ were calibrated to obtain a numerical F-CMOD curve as close as possible to the experimental outcomes (Table 4). As can be seen in Fig. 21, similar curves were obtained for 7 different parameter sets (including the primary set of parameters marked in red). The differences between the crack propagation paths are also negligible and they differ only in the rate of the softening degree of stiffness degradation of the cohesive elements (Fig. 22). It is worth noting that, for this set, the $f_{t,ITZ}/f_{t,CEM}$ ratio is almost constant and is between 0.50–0.55.

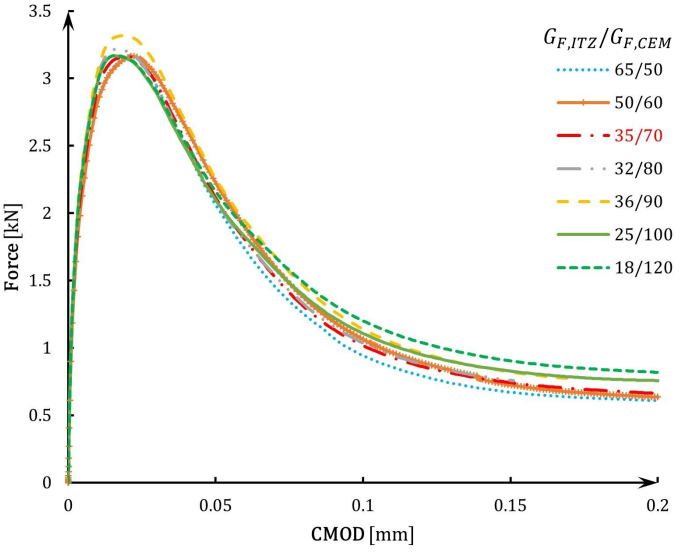

FIG. 21. F-CMOD curves for different parameters sets in constant $f_{t,CEM}$ approach for MVD.

TABLE 4. Assessment of fracture parameters for MVD test – constant $f_{t,CEM}$.

Assumed parameters		Calibrated parameters	
$f_{t,CEM}$ [MPa]	$G_{F,CEM}$ [N/m]	$f_{t,ITZ}$ [MPa]	$G_{F,ITZ}$ [N/m]
3.5	50	1.750	65
	60	1.750	51
	70	1.750	35
	80	1.750	32
	90	1.750	36
	100	1.750	25
	120	1.925	18

TABLE 5. Assessment of fracture parameters for MVD test – constant $G_{F,CEM}$.

Assumed parameters		Calibrated parameters	
$f_{t,CEM}$ [MPa]	$G_{F,CEM}$ [N/m]	$f_{t,ITZ}$ [MPa]	$G_{F,ITZ}$ [N/m]
2.5	70	2.00	31.5
3.0		1.83	38.5
3.5		1.75	35.0
4.0		1.60	35.0
4.5		1.35	31.5

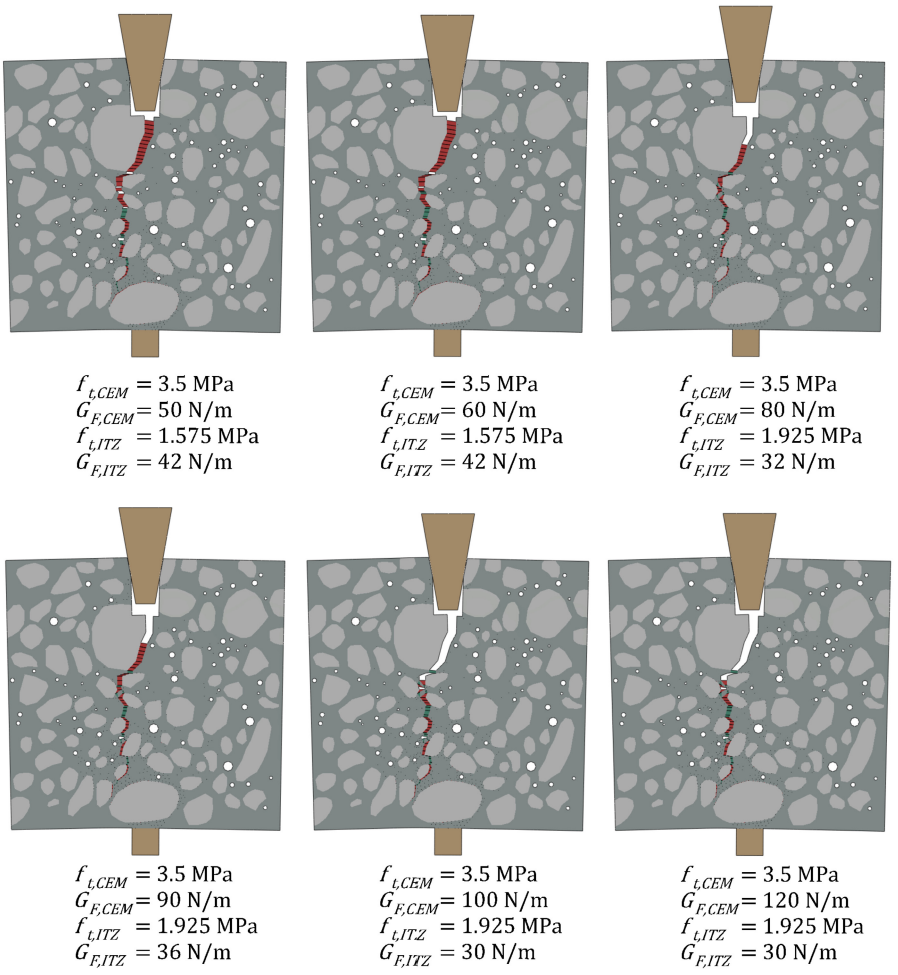

FIG. 22. Crack patterns for different parameters sets in constant $f_{t,CEM}$ approach for MVD.

The second group of parameters was obtained analogously, this time the fracture energy of the cement matrix was established as a constant parameter and the parameters of the ITZ were calibrated to the changing strength of the cement matrix (Table 5). This approach also resulted in nearly convergent F-CMOD curves with respect to the reference curve (Fig. 23). The resulting crack propagation paths also remain in high convergence with the exception of the set with the lowest $f_{t,ITZ}/f_{t,CEM}$ ratio (Fig. 24) – in this case the crack was not attracted to the interfacial zone due to its similar strength to the matrix strength. An almost constant $G_{f,ITZ}/G_{F,CEM}$ ratio between 0.45 and 0.55 was also observed for all considered sets.

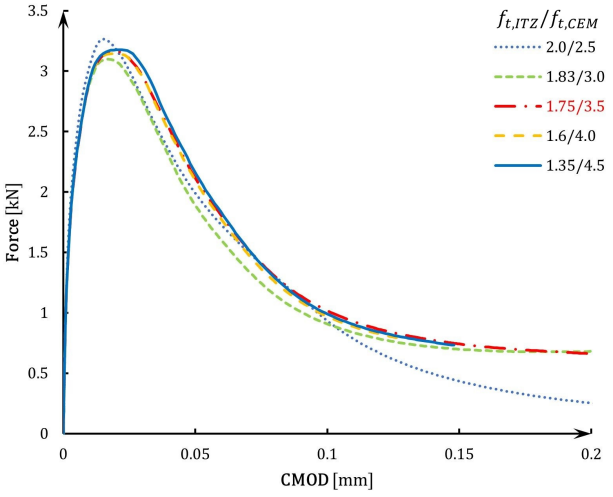

FIG. 23. F-CMOD curves for different parameters sets in constant $G_{f,CEM}$ approach for MVD.

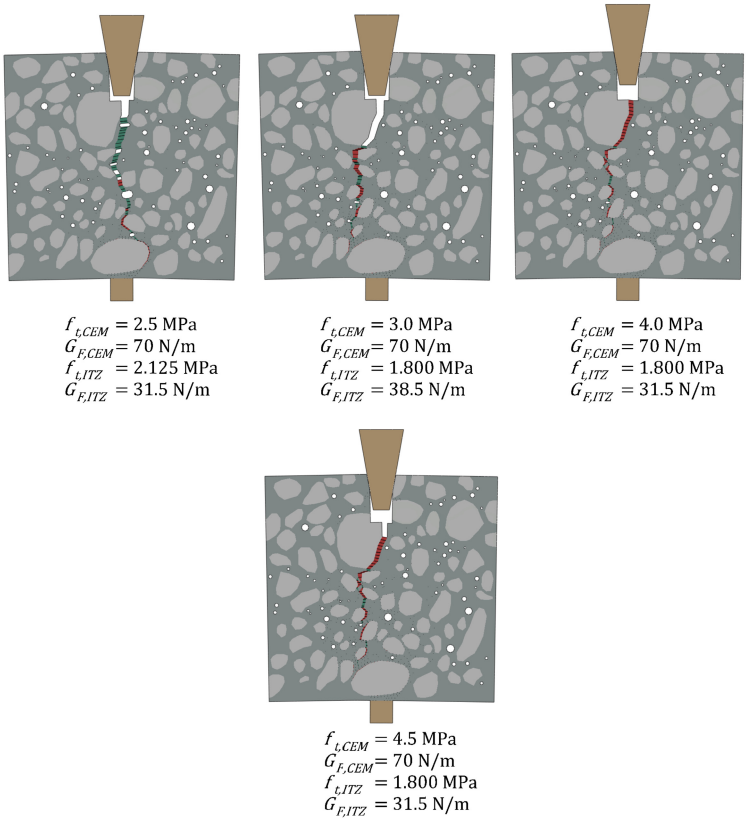

FIG. 24. Crack patterns for different parameters sets in constant $G_{f,CEM}$ approach for MVD.

5. Three-Point Bending Test

5.1. Experiment

Due to the specific conditions of the simplified MVD test: the occurrence of friction-dependent vertical stresses and the application of the load in the immediate vicinity of the crack, it was decided to carry out additional verification of the observations made in the MVD simulations. For this purpose, simulations of the three-point beam bending test described in the paper by TRAWIŃSKI *et al.* [20] were adopted. In the TPBT the loading is applied away from the crack tip. The test specimen in this case was a beam with an overall length of 320 mm and a cross-section of 40×80 mm with a notch in the central part of the lower edge of dimensions 3 mm (width) by 8 mm (height). The support spacing was 240 mm. Two beam specimens were tested experimentally, the results of the F-CMOD curves are shown in Fig. 25.

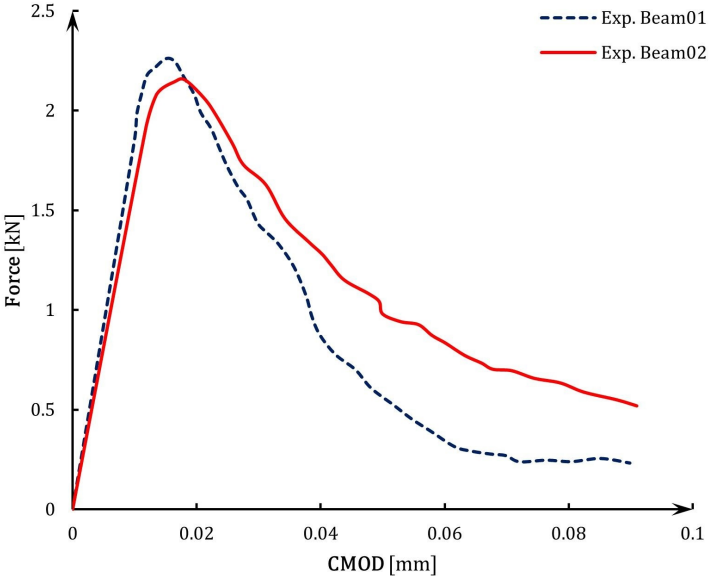

FIG. 25. Experimental F-CMOD curves for TPBT.

5.2. Input data and primary results

The input parameters (Tables 6 and 7) were taken directly from TRAWIŃSKI *et al.* [20]. A preliminary simulation was carried out on the basis of these parameters and one chosen beam mesostructure, the results of which are hereafter treated as a reference.

TABLE 6. Input parameters for bulk elements – TPBT.

Material parameter	Aggregate	Cement matrix	Homogenous part of beam
E [GPa]	47.2	29.2	36.1
ν [–]	0.2	0.2	0.2

TABLE 7. Input parameters for cohesive elements – TPBT.

Material parameter	CM-CM	ITZ
k_n^0, k_s^0 [MPa/mm]	10^6	10^6
$f_{t,n}$, $f_{t,s}$ [MPa]	4.4	1.6
α [–]	7.5	7.5
G_F [N/m]	40	20

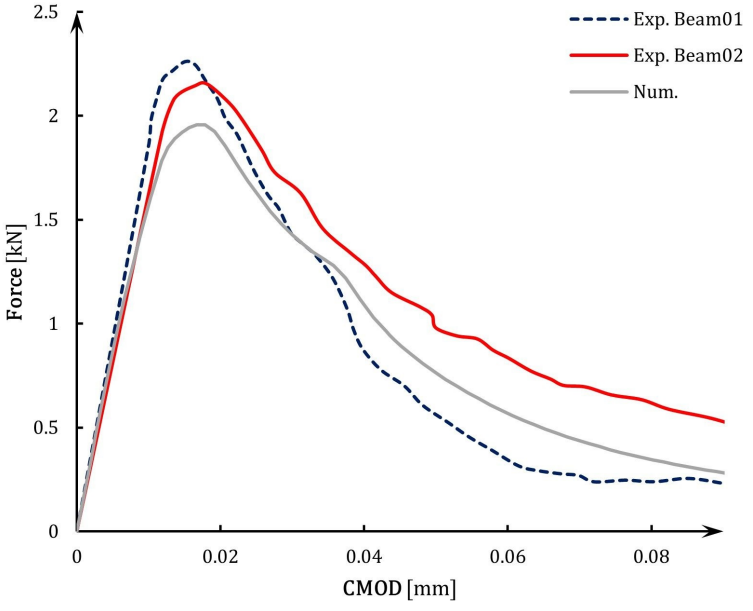

FIG. 26. Numerical obtained F-CMOD curve for TPBT vs experimental curves.

The results obtained stand in very good agreement with the experimental outcomes in terms of both the F-CMOD curves (Fig. 26) and the crack patterns (Fig. 27). In this case, the numerically obtained results are more accurate than in the MVD test simulations. In a way, this confirms the hypothesis that the numerical results of the MVD tests may be distorted by the influence of the vertical component of stress and the location of the kinematic constraint directly in the notch.

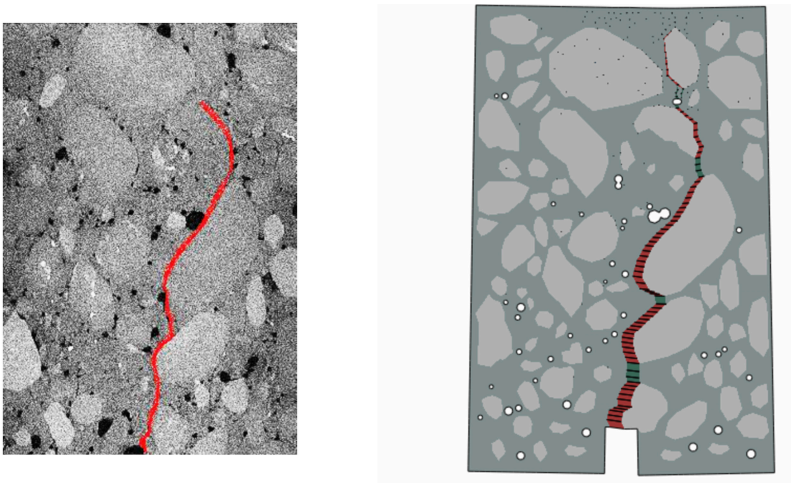

FIG. 27. Comparison of experimental and numerical obtained crack paths for primary TPBT parameters set.

5.3. Choice of parameter set

Different sets of parameters resulting in similar numerical results were also found for TPBT simulations. As before, two approaches were used – the first with a constant value of $f_{t,CEM}$ in this approach, only one set was found in addition to the main data (Figs. 28 and 29), and the second with a fixed value

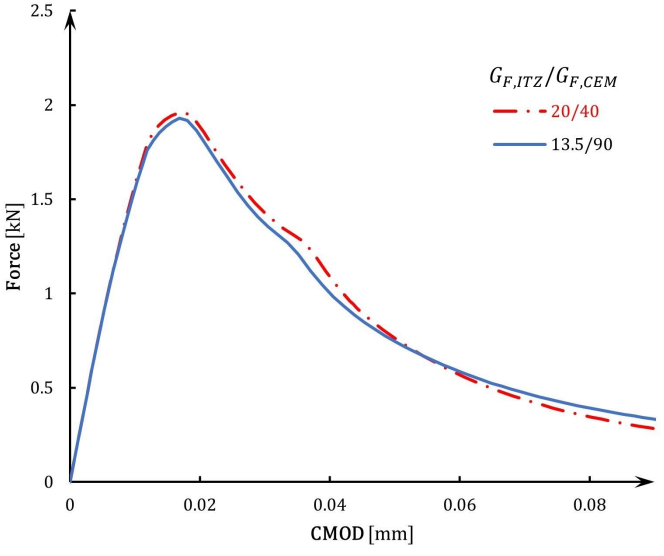

FIG. 28. F-CMOD curves for different parameters sets in constant $f_{t,CEM}$ approach for TPBT.

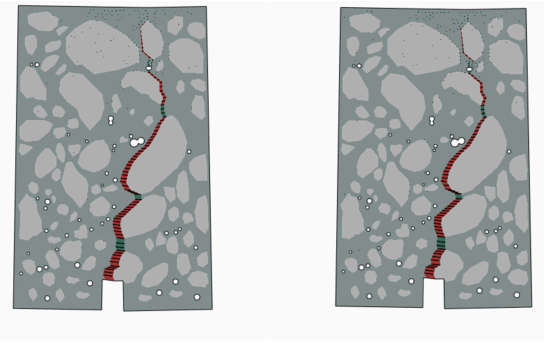

FIG. 29. Crack patterns for different parameters sets in constant $f_{t,CEM}$ approach for TPBT.

of fracture energy $G_{F,CEM}$ – in this case, 4 additional sets were found that met the assumptions (Table 8). However, this time the level of convergence of the F-CMOD (Fig. 30) results for the different parameter sets was no longer as high as for the MVD simulations. In this case, a similar relationship was also observed with $G_{F,ITZ}/G_{F,CEM}$ ratio of between 0.45 and 0.55 for all similar sets. In terms of cracking patterns (Fig. 31), a correlation analogous to that for MVD

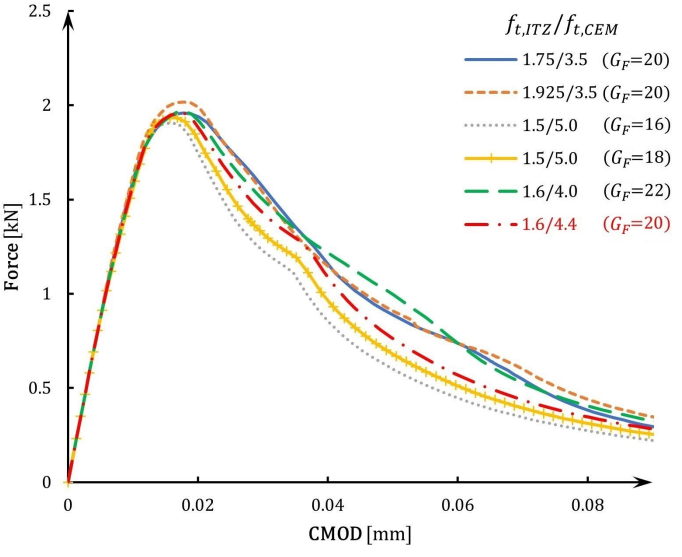

FIG. 30. CMOD curves for different parameters sets in constant $G_{f,CEM}$ approach for TPBT.

TABLE 8. Assessment of fracture parameters for TPBT – constant $G_{F,CEM}$.

Assumed parameters		Calibrated parameters	
$f_{t,CEM}$ [MPa]	$G_{F,CEM}$ [N/m]	$f_{t,ITZ}$ [MPa]	$G_{F,ITZ}$ [N/m]
3.5	40	1.750	20.0
3.5		1.925	20.0
4.0		1.600	22.0
4.4		1.600	20.0
5.0		1.500	18.0

was observed: the greater the strength of ITZs in relation to $f_{t,CEM}$ the greater is the chance of changing the trajectory of the crack because in this condition ITZ is no longer an attractor to the crack.

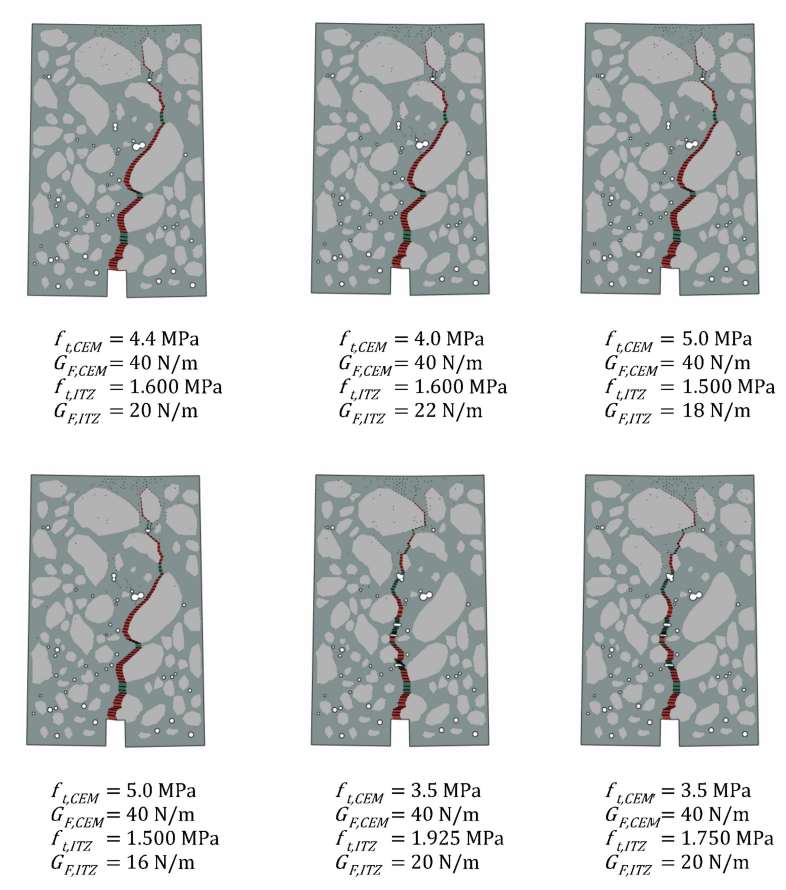

FIG. 31. Crack patterns for different parameters sets in constant $G_{f,CEM}$ approach for TPBT.

6. Conclusions

The above analyses and calculations on the impact of parameter selection of two-dimensional numerical simulations for the discrete crack propagation problem when considering the actual mesostructure result in the following conclusions:

- Without any additional information about material parameters: the tensile strength and the fracture energy for individual phases in concrete: cement matrix and interfactial transition zones, the choice of their values suffer from non-uniqueness. Numerical simulations can give the same outcome for different sets of material parameters. Moreover, uncertainty and ambiguity of choosing the uniqe set of material constants for mesoscale approach seems to strongly depend on geometry of the sample and boundary conditions.
- The use of the models based on the actual mesostructure in the simulations ensures satisfactory agreement between numerical results and experiment even though the necessary simplifications were applied. However, the observed disparities of F-CMOD curves indicate that considering 3D models may deliver more accurate results.
- In the mesoscale approach to simulate fracture phenomena in concrete obtained results strongly depend on the parameters of ITZs. Therefore, it is important to choose their mechanical parameters accordingly, and it is necessary to develop the field of numerical simulation of cracking towards an accurate estimation of ITZ parameters based on test results for homogeneous concrete.
- The execution of numerical simulations based on previously performed laboratory tests should always include complete documentation and a description of how the numerical parameters were adopted. This is not only to enable subsequent reproduction of the simulation but also to enlarge the database of parameters used, which will allow appropriate universal recommendations to be developed in the future.
- At the current state of the art, the application of detailed mesoscale numerical models requires a particularly careful selection of model parameters, supported by extended parametric studies and additional experimental data.

Acknowledgements

The FE calculations were performed at the Centre of Informatics Tricity Academic Supercomputer & Network.

References

1. J. TEJCHMAN, J. BOBIŃSKI, *Continuous and Discontinuous Modelling of Fracture in Concrete Using FEM*, Springer, Berlin, Heidelberg, 2013.
2. J. FARRAN, *Contribution minéralogique à l'étude de l'adhérence entre les constituants hydratés des ciments et les matériaux enrobés*, Review of Construction Materials (Revue des Matériaux de Construction), **490**, 155–172, 1956.
3. D.P. BENTZ, P.E. STUTZMAN, E.J. GARBOCZI, *Experimental and simulation studies of the interfacial zone in concrete*, Cement and Concrete Research, **22**, 891–902, 1992.
4. T. AKÇAOĞLU, M. TOKYAY, T. ÇELIK, *Effect of coarse aggregate size and matrix quality on ITZ and failure behavior of concrete under uniaxial compression*, Cement and Concrete Composites, **26**, 633–638, 2004.
5. M. NITKA, J. TEJCHMAN, *Meso-mechanical modelling of damage in concrete using discrete element method with porous ITZs of defined width around aggregates*, Engineering Fracture Mechanics, **231**, 107029, 2020.
6. J. WANG, A.P. JIVKOV, D.L. ENGELBERG, Q.M. LI, *Meso-scale modelling of mechanical behaviour and damage evolution in normal strength concrete*, Procedia Structural Integrity, **13**, 560–565, 2018.
7. S. ZHANG, C. ZHANG, L. LIAO, C. WANG, *Numerical study of the effect of ITZ on the failure behaviour of concrete by using particle element modelling*, Construction and Building Materials, **170**, 776–789, 2018.
8. X. HUANG, B.L. KARIHALOO, *Micromechanical modelling of the tensile behaviour of quasi-brittle materials*, [in:] W.B. Lee [ed.], *Advances in Engineering Plasticity and Its Applications*, pp. 267–272, Elsevier, Oxford, 1993.
9. A. HILLERBORG, M. MODÉER, P.-E. PETERSSON, *Analysis of crack formation and crack growth in concrete by means of fracture mechanics and finite elements*, Cement and Concrete Research, 773–782, 1976.
10. J.G. ROTS, *Smeared and discrete representations of localized fracture*, [in:] Z.P. Bažant [ed.], *Current Trends in Concrete Fracture Research*, pp. 45–59, Springer, Netherlands, Dordrecht, 1991.
11. L. JENDELE, J. ČERVENKA, V. SAOUMA, R. PUKL, *On the choice between discrete or smeared approach in practical structural FE analyses of concrete structures*, n.d.
12. R. DE BORST, J.J.C. REMMERS, A. NEEDLEMAN, M.-A. ABELLAN, *Discretevs smeared crack models for concrete fracture: bridging the gap*, International Journal for Numerical and Analytical Methods in Geomechanics, **28**, 583–607, 2004.
13. P. MENÉTREY, K.J. WILLAM, *Triaxial failure criterion for concrete and its generalization*, ACI Structural Journal, **92**, 311–318, 1995.
14. G. MESCHKE, R. LACKNER, H.A. MANG, *An anisotropic elastoplastic-damage model for plain concrete*, International Journal for Numerical Methods in Engineering, **42**, 703–727, 1998.

15. I. MARZEC, J. BOBIŃSKI, *On Some Problems in Determining Tensile Parameters of Concrete Model from Size Effect Tests*, Polish Maritime Research, **26**, 115–125, 2019.

16. Ł. SKARŻYŃSKI, I. MARZEC, A. TEJCHMAN-KONARZEWSKI, *Experiments and numerical analyses for composite RC-EPS slabs*, Computers and Concrete, **20**, 689–704, 2017.

17. Ł. SKARŻYŃSKI, I. MARZEC, K. DRĄG, J. TEJCHMAN, *Numerical analyses of novel prefabricated structural wall panels in residential buildings based on laboratory tests in scale 1:1*, European Journal of Environmental and Civil Engineering, **24**, 1450–1482, 2020.

18. R. DESMORAT, F. GATUINGT, F. RAGUENEAU, *Nonlocal anisotropic damage model and related computational aspects for quasi-brittle materials*, Engineering Fracture Mechanics, **74**, 1539–1560, 2007.

19. P. GRASSL, D. XENOS, U. NYSTRÖM, R. REMPLING, K. GYLLTOFT, *CDPM2: A damage-plasticity approach to modelling the failure of concrete*, International Journal of Solids and Structures, **50**, 3805–3816, 2013.

20. W. TRAWIŃSKI, J. BOBIŃSKI, J. TEJCHMAN, *Two-dimensional simulations of concrete fracture at aggregate level with cohesive elements based on X-ray μCT images*, Engineering Fracture Mechanics, **168**, 204–226, 2016.

21. W. TRAWIŃSKI, J. TEJCHMAN, J. BOBIŃSKI, *A three-dimensional meso-scale modelling of concrete fracture, based on cohesive elements and X-ray μCT images*, Engineering Fracture Mechanics, **189**, 27–50, 2018.

22. H. AKITA, H. KOIDE, M. TOMON, D. SOHN, *A practical method for uniaxial tension test of concrete*, Materials and Structures, **36**, 365–371, 2003.

23. D.V. PHILLIPS, Z. BINSHENG, *Direct tension tests on notched and un-notched plain concrete specimens*, Magazine of Concrete Research, **45**, 25–35, 1993.

24. F.H. WITTMANN, K. ROKUGO, E. BRÜHWILER, H. MIHASHI, P. SIMONIN, *Fracture energy and strain softening of concrete as determined by means of compact tension specimens*, Materials and Structures, **21**, 21–32, 1988.

25. A. FERNÁNDEZ-CANTELI, L. CASTAÑÓN, B. NIETO, M. LOZANO, T. HOLUŠOVÁ, S. SEITL, *Determining fracture energy parameters of concrete from the modified compact tension test*, Frattura Ed Integrità Strutturale, **8**, 383–393, 2014.

26. A. PROS, P. DÍEZ, C. MOLINS, *Numerical modeling of the double punch test for plain concrete*, International Journal of Solids and Structures, **48**, 1229–1238, 2011.

27. C. ROCCO, G.V. GUINEA, J. PLANAS, M. ELICES, *Size effect and boundary conditions in the Brazilian test: Experimental verification*, Materials and Structures, **32**, 210–217, 1999.

28. C. ROCCO, G.V. GUINEA, J. PLANAS, M. ELICES, *Size effect and boundary conditions in the Brazilian test: theoretical analysis*, Materials and Structures, **32**, 437–444, 1999.

29. M.R. KHOSRAVANI, M. SILANI, K. WEINBERG, *Fracture studies of Ultra-High Performance Concrete using dynamic Brazilian tests*, Theoretical and Applied Fracture Mechanics, **93**, 302–310, 2018.

30. N. ERARSLAN, *Analysing mixed mode (I–II) fracturing of concrete discs including chevron and straight-through notch cracks*, International Journal of Solids and Structures, **167**, 79–92, 2019.

31. P.E. PETERSON, *Fracture energy of concrete: method of determination*, Cement and Concrete Research, **10**, 79–89, 1980.

32. H. LINSBAUER, E. TSCHEGG, *Fracture energy determinationof concrete with cube specimens*, Zement Und Beton, 38–40, 1986.

33. E. BRÜHWILER, F.H. WITTMANN, *The wedge splitting test, a new method of performing stable fracture mechanics tests*, Engineering Fracture Mechanics, **35**, 117–125, 1990.

34. L. SEGURA-CASTILLO, R. MONTE, A.D. DE FIGUEIREDO, *Characterisation of the tensile constitutive behaviour of fibre-reinforced concrete: a new configuration for the Wedge Splitting Test*, Construction and Building Materials, **192**, 731–741, 2018.

35. Ł. SKARŻYŃSKI, J. SUCHORZEWSKI, *Mechanical and fracture properties of concrete reinforced with recycled and industrial steel fibers using Digital Image Correlation technique and X-ray micro computed tomography*, Construction and Building Materials, **183**, 283–299, 2018.

36. M. DI PRISCO, L. FERRARA, M.G.L. LAMPERTI, *Double edge wedge splitting (DEWS): an indirect tension test to identify post-cracking behaviour of fibre reinforced cementitious composites*, Materials and Structures, **46**, 1893–1918, 2013.

37. A. HILLERBORG, *The theoretical basis of a method to determine the fracture energy GF of concrete*, Materials and Structures, 291–296, 1985.

38. Y. YIN, Y. QIAO, S. HU, *Four-point bending tests for the fracture properties of concrete*, Engineering Fracture Mechanics, **211**, 371–381, 2019.

39. X. XIONG, Q. XIAO, *Meso-scale simulation of concrete based on fracture and interaction behavior*, Applied Sciences, **9**, 2986, 2019.

40. J. YING, J. GUO, *Fracture behaviour of real coarse aggregate distributed concrete under uniaxial compressive load based on cohesive zone model*, Materials, **14**, 4314, 2021.

41. B. KONDYS, J. BOBIŃSKI, I. MARZEC, *Numerical investigations of discrete crack propagation in Montevideo splitting test using cohesive elements and real concrete micro-structure*, [in:] Computational Modelling of Concrete and Concrete Structures, pp. 107–116, CRC Press, London, 2022.

42. T.J. TRUSTER, *DEIP, discontinuous element insertion Program – Mesh generation for interfacial finite element modeling*, SoftwareX, **7**, 162–170, 2018.

43. P.-E. PETERSSON, *Crack Growth and Development of Fracture Zones in Plain Concrete and Similar Materials*, Lund Institute of Technology, Lund, 1981.

44. G.I. BARENBLATT, *The mathematical theory of equilibrium cracks in brittle fracture*, Advances in Applied Mechanics, **7**, 55–129, 1962.

45. W. REN, Z. YANG, R. SHARMA, C. ZHANG, P.J. WITHERS, *Two-dimensional X-ray CT image based meso-scale fracture modelling of concrete*, Engineering Fracture Mechanics, **133**, 24–39, 2015.

46. Ł. SKARŻYŃSKI, M. NITKA, J. TEJCHMAN, *Modelling of concrete fracture at aggregate level using FEM and DEM based on X-ray μCT images of internal structure*, Engineering Fracture Mechanics, **147**, 13–35, 2015.

47. X. XI, Z. YIN, S. YANG, C.-Q. LI, *Using artificial neural network to predict the fracture properties of the interfacial transition zone of concrete at the meso-scale*, Engineering Fracture Mechanics, **242**, 107488, 2021.

48. B.G. RABBAT, H.G. RUSSELL, *Friction coefficient of steel on concrete or grout*, Journal of Structural Engineering, **111**, 505–515, 1985.

Received November 30, 2022; revised version April 26, 2023.
Published online June 22, 2023.